TISSUE ENGINEERING: Part A
Volume 22, Numbers 21 and 22, 2016

DOI: 10.1089/ten.tea.2016.0149

termis
Tissue Engineering
& Regenerative Medicine
International Society

ORIGINAL ARTICLE

In Vivo Cellular Infiltration and Remodeling in a Decellularized Ovine Osteochondral Allograft

Tyler Novak, PhD,[1] Kateri Fites Gilliland, MS,[1] Xin Xu, PhD,[1,2] Logan Worke, MS,[1] Aaron Ciesielski, BS,[3] Gert Breur, DVM, PhD,[4] and Corey P. Neu, PhD[1,2]

Interest in decellularized tissues has steadily gained as potential solutions for degenerative diseases and traumatic events, replacing sites of missing tissue, and providing the relevant biochemistry and microstructure for tissue ingrowth and regeneration. Osteoarthritis, a progressive and debilitating disease, is often initiated with the formation of a focal defect in the otherwise smooth surface of articular cartilage. Decellularized cartilage tissue, which maintains the structural complexity of the native extracellular matrix, has the potential to provide a clinically relevant solution to focal defects or large tissue damage, possibly even circumventing or complementing current techniques such as microfracture and mosaicplasty. However, it is currently unclear whether implantation of decellularized cartilage *in vivo* may provide a mechanically and biochemically relevant platform to promote cell remodeling and repair. We examined whole decellularized osteochondral allografts implanted in the ovine trochlear groove to investigate cellular remodeling and repair tissue quality compared to empty defects and contralateral controls (healthy cartilage). At 3 months postsurgery, cells were observed in both the decellularized tissue and empty defects, although both at significantly lower levels than healthy cartilage. Qualitative and quantitative histological analysis demonstrated maintenance of cartilage features of the decellularized implant similar to healthy cartilage groups. Noninvasive analysis by quantitative magnetic resonance imaging showed no difference in $T_{1\rho}$ and T_2* between all groups. Investigation of the mechanical properties of repair tissue showed significantly lower elasticity in decellularized implants and empty defects compared to healthy cartilage, but similar tribological quantities. Overall, this study suggests that decellularized cartilage implants are subject to cellular remodeling in an *in vivo* environment and may provide a potential tissue engineering solution to cartilage defect interventions.

Keywords: decellularization, cartilage tissue engineering, cell remodeling and regeneration, recellularization, defect repair

Introduction

The local extracellular matrix (ECM) is critical in directing form and function of the local cell population. Continuous feedback mechanisms between the local cell population and ECM serve to maintain the structural and biochemical composition of the native tissue.[1,2] Alterations in the ECM structure, beyond a critical size, incurred by either traumatic injury or biochemical changes can introduce a cascade effect leading to the development of a disease state in the tissue.[2,3] This is especially prevalent in tissue such as articular cartilage, which is populated with a low density of semiquiescent chondrocytes known for poor regeneration of damaged tissue.[3] Weakening of the cartilage tissue structure can result in the formation of a local defect, which can act as the genesis point for progressive inflammation and wear, eventually leading to total degradation of the tissue and clinical osteoarthritis (OA), which currently affects over 27 million Americans.[2,4,5] A regenerative medicine intervention at the local defect level has the potential to mitigate the progression of long-term OA. The role of the ECM and cell–matrix interactions have been well recognized for the regeneration potential of cartilage defects with autologous chondrocytes as well as stem cell sources.[1,2,6,7] Currently, the structural and biochemical complexity of mature cartilage is unable to be reproduced *in vitro*.[2] Such tissue engineering approaches have been successful in emulating specific characteristics of the native cartilage structure, such as fibril

[1]Weldon School of Biomedical Engineering, Purdue University, West Lafayette, Indiana.
[2]Department of Mechanical Engineering, University of Colorado Boulder, Boulder, Colorado.
[3]Purdue University-North Central, Westville, Indiana.
[4]Department of Veterinary Clinical Sciences, Purdue University, West Lafayette, Indiana.

anisotropy and local mechanical properties, but still require further modifications to produce a truly equivalent structure to native cartilage.[8–10] As a result, researchers have used the potential of tissue decellularization as a source of healthy cartilage tissue potentially useful for driving repair.[6,7]

The use of the native cartilage structure is additionally in clinical use, although without the use of decellularization. Current surgical methods for the repair of cartilage defects by ECM replacement include osteochondral autograft transfer system and mosaicplasty.[2,3] Both of these methods involve the harvest of cellularized articular cartilage autografts from relatively low load-bearing regions to fill the defect and promote regeneration of the tissue and have the advantage of delivering autologous cells to the center of the defect. However, these methods often introduce significant surgical site comorbidity and can cause an inflammatory response, hindering tissue repair and potentially inducing an OA cascade.

Decellularized ECM constructs, however, lower the potential for an immunogenic response, allowing for the use of allogenic or xenogenic tissue, and minimize the surgical risk to the patient.[2,3,11] Outside of articular cartilage, decellularized materials represent a significant portion of clinically available tissue engineering solutions.[2] However, articular cartilage is characteristically dense and has been shown to restrict cellular infiltration over the course of weeks in both *in vitro* studies and *in vivo* subcutaneous trials.[12–16] Specifically, it has been noted that cell infiltration is limited by substrate stiffness as well as the ratio of pore size to nucleus cross sectional area, where infiltration was not found to take place in pores smaller than 10% of the nucleus cross sectional area.[17,18] Without cellular infiltration or remodeling, integration of the donor tissue is less likely and can result in susceptibility of the implant to degradation and minimized utility as a long-term solution to local cartilage defects.[19] Researchers have attempted to circumnavigate this issue through the utility of chemical treatments to increase the porosity of the native tissue, utilize decellularized fragments to create porosity from particle packing inefficiencies, and create thin cell/ECM sandwich structures.[3,19–21] Unfortunately, none of these solutions, including decellularized cartilage tissue without porosity modification, have shown to achieve significant cellular infiltration or remodeling in both *in vitro* and *in vivo* studies.[2,3]

However, several of the initial conditions of these previous studies are potentially limiting factors to driving cellular remodeling. First, decellularized cartilage samples are often hydrated with sterile, isotonic solution before cellular seeding or implantation, limiting internal swelling pressures that may facilitate incorporation of cells or soluble chemotactic signals. In addition, previous *in vivo* studies have placed these implants in subcutaneous locations, limiting their exposure to the native, autologous cell source, the native biochemical microenvironment (e.g., growth factors), and to the complex mechanical environment experienced in articular joints.[3,6,11,16,19] Each of these factors has been shown to contribute to cartilage regeneration and phenotype expression *in vitro* and are likely important to the *in vivo* regeneration potential as well.[7] Clinically relevant exposure to these three important facets of implant survival and regenerative potential is necessary to investigate the limitations of cellular remodeling in the dense articular cartilage in a way that can be clinically relevant to the survival and potential success of the implant. Our study attempts to address this issue by utilizing decellularized, lyophilized, but otherwise unmodified, whole cartilage tissue in an established, critical size osteochondral defect model (ovine) that is clinically similar to the human population and of greater size than those seen to previously successfully observed cell remodeling *in vivo*. This study was designed to meet the following objectives: (1) show effective decellularization and minimal biochemical alteration of whole osteochondral tissue, (2) investigate the cellular remodeling capability of whole decellularized tissue in a critical size implant over a 3-month period after *in vivo* implantation, and (3) observe and measure the maintenance in tissue quality and potential remodeling as a result of cell remodeling compared to empty defects and contralateral healthy cartilage.

Materials and Methods

Explant extraction and decellularization

Ovine osteochondral explants (ø = 6 mm, thickness = 10 mm, $n = 6$) were acquired from six animals (aged <3 years.) in an aseptic environment. Joints were acquired from a local abattoir within 24 h of sacrifice. Cylindrical osteochondral (donor) tissues were harvested from standardized locations (Fig. 1) of the trochlear groove using a coring reamer (Arthrex, Inc., Naples, FL). Samples were immediately decellularized following harvest.

Donor tissues were decellularized as previously described.[22] Briefly, samples were incubated at 37°C in sterile 2% sodium dodecyl sulfate (SDS; Sigma, St. Louis, MO) in 1× phosphate-buffered saline (PBS) with agitation for 24 h. Following sterile 1× PBS rinsing, samples were immediately frozen at −80°C. Before implantation, samples were lyophilized for 24 h for complete removal of interstitial fluid. DNase was not utilized in this study, as previous work has found SDS treatment to adequately remove genetic material from articular cartilage.[11,14]

Hydroxyproline and dimethylmethylene blue analysis

To examine the effect of decellularization on the biochemical composition of the explant, a separate study was performed examining collagen and glycosaminoglycan (GAG) content. Ovine tibiofemoral and patellofemoral joints were obtained from a local abattoir within 24 h of sacrifice. From each joint, osteochondral explants (ø = 5 mm, thickness = 1.5 mm) were acquired from five separate animals in the trochlear groove and site matched to the intended donor locations. Samples were acquired and paired bilaterally from two locations in the trochlear groove using a coring reamer at proximal and distal locations (Fig. 1). Laterally paired samples were randomly assigned to either control (healthy cartilage) or treatment groups, with the corresponding sample placed in the opposite group. Samples were immediately frozen to −80°C until testing. Decellularized samples were similarly thawed and decellularized in 2% SDS solution at 37°C for 24 h, identical to implanted samples. Collagen content of decellularized and healthy cartilage samples ($n = 7$) was assessed using a hydroxyproline assay kit (Sigma) as per manufacturer's instructions, and compared to a hydroxyproline standard as previously described.[23] GAG content of decellularized and healthy cartilage samples ($n = 10$) was determined by dimethylmethylene blue (DMMB) assay, as previously described.[24]

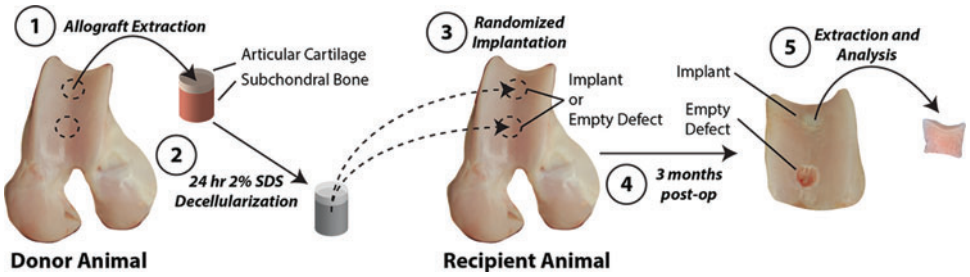

FIG. 1. Donor and recipient animals of similar age/weight were utilized to investigate cellular remodeling into decellularized osteochondral explants implanted *in vivo*. Donor osteochondral tissues were removed from freshly slaughtered sheep at the trochlear groove (proximal and distal locations), decellularized for 24 h (sterile 2% sodium dodecyl sulfate [SDS] solution), and thoroughly rinsed. Donor tissue was randomly implanted (balanced randomization) in distal or proximal regions of the trochlear groove and matched to the local curvature of the articular surface. Within the same joint, the alternate location was left as an empty defect, as a negative control. Three months postoperatively, implants and surrounding tissues were harvested and separated for analysis. Color images available online at www.liebertpub.com/tea

Ovine implantation and extraction

Following institutional approval, sample implantation occurred over 3 days, with two animals performed per day. As previously stated, all donor tissues were sourced from ovine trochlear groove, site matched to the intended recipient site, decellularized using the described protocol, and lyophilized before implantation. All surgeries were performed on the right leg, with the opposing leg to serve as a contralateral control (healthy cartilage). A total of two defects were created at proximal and distal locations in the trochlear groove (Figs. 1 and 2b). For each defect, a guide wire was placed normal to surface to ensure consistency in implant fitting into the defect. Initial defects of 6 mm diameter and 5 mm depth were created utilizing the guide wire. Subsequently, defects were cut to a final depth of 10 mm utilizing a custom end mill system. Decellularized samples were then randomly (location balanced, $n = 3$ for each location) press-fit into the proximal or distal defect. Locations that did not receive an implant served as empty defects (Fig. 2b). We additionally note that defects were also created in the condyles to evaluate collagen matrix-based repair in a parallel study. Histological analysis between defects in the condyle and trochlear groove was similar, suggesting no interaction between condyle defects and therefore minimized impact on the outcomes presented herein.

Ovine joints were recovered after the duration of the 12-week study within 3 h of sacrifice. All locations on the experimental and contralateral control joint were removed using a 10 mm coring reamer (Arthrex, Inc.) to include the defect as well as surrounding native tissue. After removal, samples were cut in half vertically in the medial–lateral plane where one half was used for cell viability/quantitative magnetic resonance imaging (qMRI)/mechanical analysis and the other half for histological analysis.

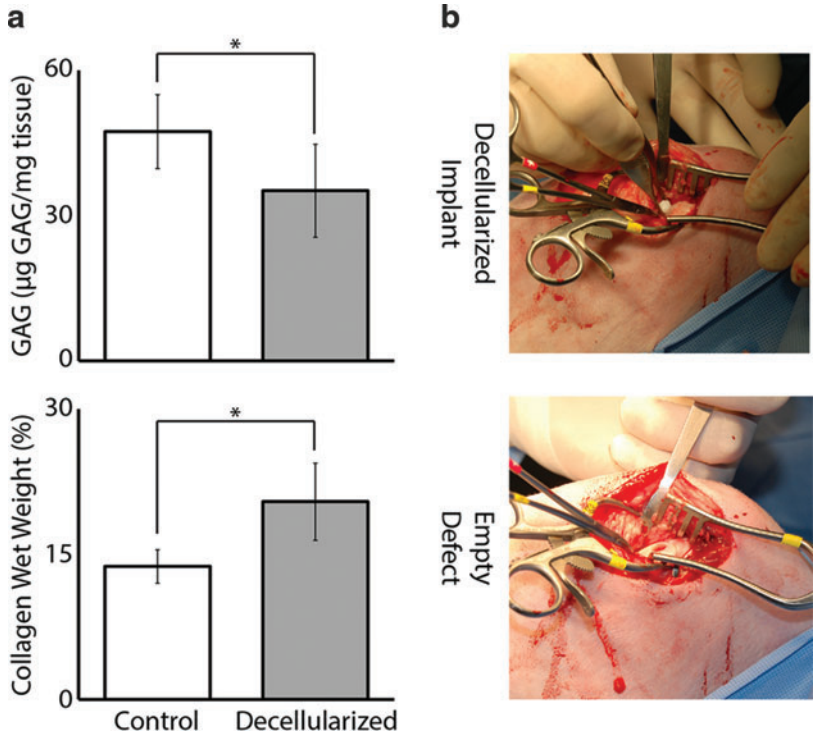

FIG. 2. SDS decellularization methods before implantation led to slight alterations in biochemical makeup of donor tissues. **(a)** Dimethylmethylene blue and hydroxyproline analysis showed a decrease in overall glycosaminoglycan (GAG) content as well as an increase in wet-weight collagen content. **(b)** Examples of surgical procedure and implant handling. Donor tissues were press-fit into similar sized defects, which were formed by a drilling process 1 cm deep, matching the dimensions of the implant and accessing the underlying marrow space in a manner similar to microfracture. (*$p < 0.05$). Color images available online at www.liebertpub.com/tea

Cellular remodeling and viability

Immediately after harvest, cartilage halves for cell viability analysis were immersed in DMEM/F12 media containing calcein and propidium iodide for cell viability and cellular remodeling analysis. After 15 min of incubation in staining solution, samples were immediately imaged by fluorescence microscopy (Nikon Eclipse Ti Widefield Microscope, 10× magnification) over the entire cut surface to include the interface region between implant/defect and native cartilage. Cell viability was quantified by particle analysis in ImageJ for each channel using a size bandwidth threshold to eliminate error from possible channel bleedover. Cellular remodeling was determined for the number of cells that had reached the center (inner 1/3rd of the implant/defect) versus the edge (outer 1/3rd). The magnitude of cells in each region was then compared to average cell density in the contralateral healthy cartilage samples.

Histological analysis

After harvest from the joints, half-samples were immediately placed in Bouin's Solution and fixed for 24 h. Samples were subsequently transferred to 70% ethanol solution for 2 weeks, with ethanol changes every 2 days. Samples were subsequently sent to the Purdue Histology and Phenotyping Laboratory for paraffin fixation, and subsequent sectioning and staining were performed at an offsite location (Cook Research, Inc., West Lafayette, IN). Separate sections were stained with H&E and Safranin O to examine gross morphology as well as articular cartilage markers.

Histological differences and potential damage that may have impacted the recellularization process were analyzed. Specifically, the International Cartilage Repair Society II scoring paradigm was utilized to investigate the structural and histological state of the samples.[25] Scoring was performed by two individuals blinded to the experimental group.

qMRI analysis

Bulk tissue structure was noninvasively analyzed by standard and quantitative MRI. Tissue assessments by qMRI included $T_{1\rho}$, a time relaxation parameter known to be influenced by water and proteoglycan content, and T_2*, a time relaxation parameter sensitive to water and the collagen fiber network.[26,27] Healthy cartilage and implant tissues were scanned using a 7.0 Tesla (T) MRI system (Bruker Medical GMBH) using an 86 mm (transmit) RF coil and 20 mm (receive) surface coil placed adjacent to the cut surface. Tissue morphology was visualized using a fast low-angle shot (FLASH) imaging sequence to acquire 3D (2D multislice) volume images. FLASH parameters were as follows: TE/TR = 4.0/146.0 ms; in-plane spatial resolution = $78 \times 78\ \mu m^2$; image matrix size = 256×256 pixels^2; number of averages = 1; slice thickness = 0.5 mm; number of slices = 15; and flip angle = 30°. In a single image slice defined from the FLASH volume image, spatial (pixel-by-pixel) maps of $T_{1\rho}$ and T_2* relaxation times were acquired. $T_{1\rho}$ imaging parameters were as follows: TE/TR = 7.9/1062.5 ms; number of averages = 8; spin-lock strength = 42.4 μT; and spin-lock durations = [10, 20, 30, 40, 50] ms. T_2* imaging parameters were as follows: TE/TR = 2.6/369.9 ms; number of averages = 8; number of echo images = 6; echo spacing = 2.8 or 3.5 ms; and flip angle = 30°. Relaxation times were determined using a monoexponential curve-fitting algorithm in MATLAB (The Mathworks, Natick, MA) and regions of interest defined by the middle third (center, repair) and outer third (side, repair to healthy cartilage interface) of the cartilage repair tissue.

Mechanical analysis

A Keysight 5500 AFM system (Keysight Technologies Inc., Santa Rosa, CA) was used to evaluate the surface roughness, fiction coefficient, and compressive modulus of the sheep articular cartilage, following previous studies from our laboratory.[28,29] To ensure accurate model fitting, a cantilever with a 5 μm borosilicate glass sphere attached to the free end (NovaScan Technologies, Inc., Ames, IA) was used, and the cantilever stiffness was calibrated as 0.07 N/m by the thermal calibration method.[30] The tissues were affixed with cyanoacrylate to a Petri dish with the articular surface facing upward, and immersed in PBS for atomic force microscopy (AFM) testing. Each plug was scanned at three different locations at center (repaired area) and three locations at the edge (native tissue area) of the articular surface. At each location, a contact mode scan with an in-plane resolution of $0.24 \times 0.24\ \mu m^2$ (scan size = $30 \times 30\ \mu m^2$; matrix = 128×128 pixels^2), scan speed 1 line/s, and set point force about 10.23 nN was first performed to acquire surface roughness and friction coefficient. Root-mean-square (RMS) surface roughness was obtained using WSxM software[31] after the surface tilt was corrected; and the lateral force calibration was determined to be 48.43 nN/V.[32] Then, individual microindentations, that is, force–distance curves, were acquired at the four corners of each scan area (i.e., 12 locations per sample) with a trigger force of 17.06 nN and load/unload speed of 4 μm/s. A Hertz contact model was fit into the indentation curves to extract the compressive modulus.[33]

Statistical analysis

A paired *t*-test between corresponding control (healthy cartilage) and treatment (decellularized) explants was utilized for both hydroxyproline and DMMB assays. Histological scoring, quantitative MRI measures, and AFM measures were all analyzed by general linear method (GLM) analysis of variance (ANOVA) with main effects of treatment and anatomical location, including interaction, as well as separate animals treated as a random effect. Cell viability was assessed by a similar GLM ANOVA with an added level of edge versus middle to assess remodeling. All *post-hoc* analysis was done by Dunnett's test, where contralateral healthy cartilage samples were treated as the comparative control. All significance restricted to $p < 0.05$. All values reported as mean ± standard deviation.

Results

SDS decellularization alters ECM composition

Decellularized explants showed a significant increase ($p = 0.004$) in relative wet-weight percentage of collagen content from healthy cartilage (13.7% w/w) to decellularized (20.4% w/w) samples. GAG content was found to significantly decrease with SDS decellularization ($p = 0.013$) from healthy cartilage (47.3 μg/mg of cartilage) to decellularized (25.2 μg/mg of cartilage) samples (Fig. 2a).

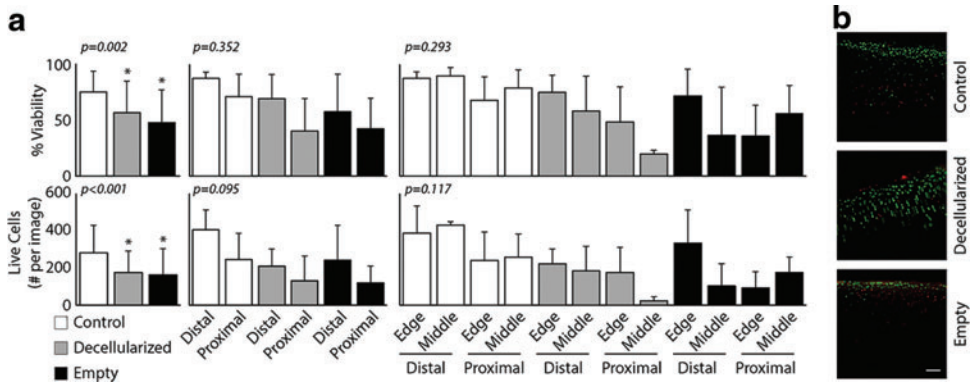

FIG. 3. Cellular remodeling occurred in all tissues, with viable cells reaching the interior (*middle*) of the decellularized donor tissue or defect repair equally well as near the edge (cell source). **(a)** Cell viability and the number of alive cells (per image) were found to be significantly higher in contralateral controls compared to both decellularized implants and empty defects ($*p < 0.001$ for both). Although not significant, distal locations were observed with higher viability and total live cell number. In addition, no significant difference was seen in either measure examining cell viability closest (*edge*) or furthest (*middle*) from the native tissue, suggesting cellular remodeling within the entire implant. **(b)** Representative examples of live/dead images (*green* = live cells, *red* = dead cell nuclei) showed distribution of live and dead cells across the experimental groups (all images representative of center of implant/defect/control). White scale bar = 100 μm. Color images available online at www.liebertpub.com/tea

Native chondrocytes remodel decellularized cartilage implants

Viability measurements reveal significant differences between treatments for overall cell viability ($p = 0.002$) and number of live cells in the implant region ($p < 0.001$), as well as significance of the anatomical location effect for cell viability ($p = 0.036$) and number of live cells ($p = 0.002$) (Fig. 3a). No significance was seen for the edge versus middle effect, any interaction, or the random animal effect ($p > 0.200$ for all). Dunnett's tests showed that healthy cartilage samples were found to have significantly higher viability and number of live cells than both decellularized implants and empty defects ($p < 0.05$ for both). However, we note that the number of cells within decellularized implant and empty defects was well above zero, but approximately half that of healthy tissue (Fig. 3a). Qualitatively, we observed cellular remodeling at the surface and within the interior of the tissue at the middle and edges of the decellularized implants and empty defects (Fig. 3b).

Decellularized cartilage retains histological features of native cartilage

Histological analysis revealed differences between each experimental group (healthy cartilage, decellularized implant, and empty defect). Contralateral healthy cartilage samples were shown to exhibit relatively thick cartilage with

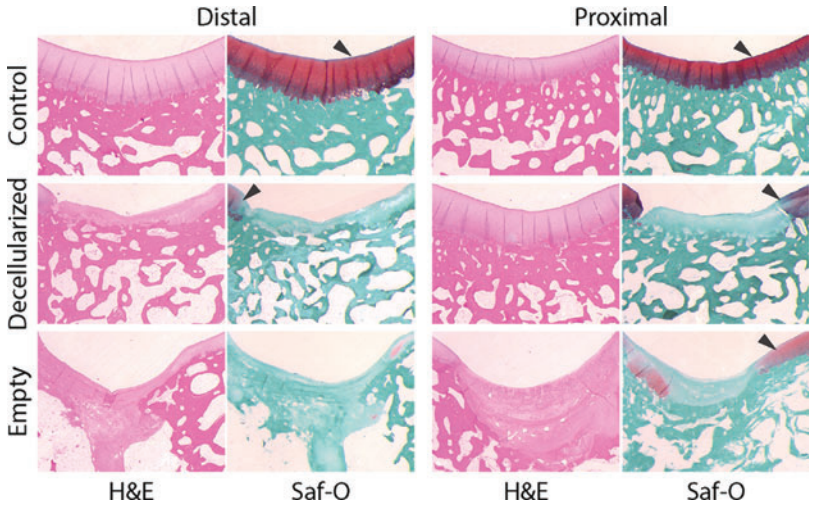

FIG. 4. Histological staining showed qualitative similarities between decellularized donor tissues and control samples. Decellularized implants and control samples showed similar surface features, while decellularized implants lacked strong proteoglycan/GAG staining (Safranin-O [Saf-O]). In addition, decellularized implants retained the osteochondral tidemark and exhibited lateral and basal integration of the implant. Empty defects show significant fibrosis, atypical surface features, and invasion into the bone space. Similar to other measures performed, distal decellularized implants exhibited more consistent cartilage features and Saf-O staining similar to controls. *Arrowheads* mark Saf-O-stained areas of interest. H&E, hematoxylin and eosin. Color images available online at www.liebertpub.com/tea

Table 1. Mean Scores and Statistical Results for International Cartilage Repair Society II Scoring Data

ICRS II category	*Treatment*	*Location*	*Score*	p-*Values*	
Tissue morphology	Control	Distal	83.33 ± 24.25	Treatment	$p = 0.002$
	Control	Proximal	98.33 ± 5.77		
	Decellularized	Distal	83.33 ± 16.33	Location	$p = 0.391$
	Decellularized	Proximal	46.70 ± 28.00		
	Empty	Distal	43.33 ± 24.43	Interaction	$p = 0.062$
	Empty	Proximal	46.30 ± 22.90		
Matrix staining	Control	Distal	85.00 ± 32.82	Treatment	$p = 0.021$
	Control	Proximal	92.08 ± 5.77		
	Decellularized	Distal	50.00 ± 42.90	Location	$p = 0.633$
	Decellularized	Proximal	53.30 ± 25.00		
	Empty	Distal	30.00 ± 32.90	Interaction	$p = 0.629$
	Empty	Proximal	45.00 ± 26.50		
Cell morphology	Control	Distal	86.67 ± 31.14	Treatment	$P = 0.002$
	Control	Proximal	97.50 ± 8.66		
	Decellularized	Distal	70.00 ± 25.30	Location	$p = 0.940$
	Decellularized	Proximal	76.67 ± 20.66		
	Empty	Distal	31.70 ± 29.90	Interaction	$p = 0.774$
	Empty	Proximal	22.50 ± 26.30		
Cell clustering	Control	Distal	88.33 ± 22.90	Treatment	$p = 0.013$
	Control	Proximal	95.83 ± 7.93		
	Decellularized	Distal	56.70 ± 41.30	Location	$p = 0.814$
	Decellularized	Proximal	60.00 ± 36.90		
	Empty	Distal	35.00 ± 40.40	Interaction	$p = 0.949$
	Empty	Proximal	35.00 ± 47.30		
Surface architecture	Control	Distal	86.67 ± 27.08	Treatment	$p = 0.013$
	Control	Proximal	95.83 ± 6.69		
	Decellularized	Distal	60.00 ± 32.90	Location	$p = 0.526$
	Decellularized	Proximal	57.50 ± 24.80		
	Empty	Distal	40.00 ± 25.30	Interaction	$p = 0.644$
	Empty	Proximal	58.80 ± 23.20		
Basal integration	Control	Distal	89.17 ± 23.14	Treatment	$p = 0.005$
	Control	Proximal	100.00 ± 0.00		
	Decellularized	Distal	90.00 ± 8.94	Location	$p = 0.599$
	Decellularized	Proximal	55.00 ± 36.20		
	Empty	Distal	38.30 ± 29.90	Interaction	$p = 0.147$
	Empty	Proximal	50.00 ± 29.40		
Tidemark	Control	Distal	88.33 ± 25.88	Treatment	$p = 0.005$
	Control	Proximal	98.33 ± 5.77		
	Decellularized	Distal	80.00 ± 16.73	Location	$p = 0.839$
	Decellularized	Proximal	76.67 ± 20.66		
	Empty	Distal	48.30 ± 34.30	Interaction	$p = 0.567$
	Empty	Proximal	40.00 ± 29.40		
Bone abnormalities	Control	Distal	91.67 ± 19.92	Treatment	$p = 0.001$
	Control	Proximal	100.00 ± 0.00		
	Decellularized	Distal	83.33 ± 13.66	Location	$p = 0.597$
	Decellularized	Proximal	53.30 ± 40.80		
	Empty	Distal	33.33 ± 20.66	Interaction	$p = 0.228$
	Empty	Proximal	41.30 ± 36.60		
Inflammation	Control	Distal	99.17 ± 2.887	Treatment	$p = 0.001$
	Control	Proximal	100.00 ± 0.00		
	Decellularized	Distal	100.00 ± 0.00	Location	$p = 0.083$
	Decellularized	Proximal	100.00 ± 0.00		
	Empty	Distal	93.33 ± 8.16	Interaction	$p = 0.209$
	Empty	Proximal	97.50 ± 5.00		
Abnormal calcification	Control	Distal	98.33 ± 3.89	Treatment	$p = 0.007$
	Control	Proximal	99.17 ± 2.89		
	Decellularized	Distal	81.67 ± 21.37	Location	$p = 0.881$
	Decellularized	Proximal	63.30 ± 31.40		
	Empty	Distal	53.30 ± 37.20	Interaction	$p = 0.392$
	Empty	Proximal	75.50 ± 22.20		

(*continued*)

Table 1. (Continued)

ICRS II category	*Treatment*	*Location*	*Score*	p-*Values*	
Vascularization	Control	Distal	99.17 ± 2.89	Treatment	$p = 0.015$
	Control	Proximal	99.17 ± 2.90		
	Decellularized	Distal	83.33 ± 16.33	Location	$p = 0.362$
	Decellularized	Proximal	55.00 ± 27.40		
	Empty	Distal	56.70 ± 45.00	Interaction	$p = 0.607$
	Empty	Proximal	50.00 ± 57.70		
Superficial assessment	Control	Distal	89.58 ± 19.82	Treatment	$p = 0.001$
	Control	Proximal	99.17 ± 2.89		
	Decellularized	Distal	77.50 ± 18.37	Location	$p = 0.271$
	Decellularized	Proximal	43.30 ± 35.60		
	Empty	Distal	43.30 ± 36.70	Interaction	$p = 0.168$
	Empty	Proximal	35.00 ± 28.90		
Mid/deep zone assessment	Control	Distal	89.17 ± 23.14	Treatment	$p = 0.002$
	Control	Proximal	100.00 ± 0.00		
	Decellularized	Distal	85.00 ± 15.17	Location	$p = 0.404$
	Decellularized	Proximal	55.00 ± 39.40		
	Empty	Distal	40.00 ± 31.00	Interaction	$p = 0.201$
	Empty	Proximal	35.00 ± 33.20		
Overall assessment	Control	Distal	88.75 ± 22.97	Treatment	$p = 0.003$
	Control	Proximal	98.33 ± 3.89		
	Decellularized	Distal	82.50 ± 15.41	Location	$p = 0.339$
	Decellularized	Proximal	50.80 ± 36.80		
	Empty	Distal	42.50 ± 34.30	Interaction	$p = 0.191$
	Empty	Proximal	36.30 ± 30.40		

ICRS II, International Cartilage Repair Society II.

features typical to the native state, including the presence of a tidemark, zonal collagen structure, proteoglycan staining by Safranin-O, and clear transition in the osteochondral region without bone invasion into the cartilage tissue (Fig. 4). Similarly, many of these features were largely retained in decellularized implants. Repaired cartilage tissue in decellularized implants retained features such as the tidemark, zonal collagen structure, and minimal bone invasion into the tissue, but lacked strong Safranin-O staining in the cartilage section of the matrix (Fig. 4). Alternatively, empty defect samples were found to exhibit very little morphological similarities to native articular cartilage (Fig. 4). Thickness of cartilage regions was not found to be significant between treatment groups ($p = 0.200$). Significant fibrosis and bone invasion into the tissue were found with little formation of tidemark separation between the two tissue types. Minimal Safranin-O staining was found in the empty defect regions.

Histological features were further quantified for all samples by International Cartilage Repair Society (ICRS) II Scoring Assessment for the quality of cartilage repair (Table 1 and Fig. 5). Treatment was found to be significant for all measurements: tissue morphology ($p = 0.002$), matrix staining ($p = 0.021$), cell morphology ($p = 0.002$), cell clustering ($p = 0.013$), surface architecture ($p = 0.013$), basal integration ($p = 0.005$), tidemark formation ($p = 0.005$), bone abnormalities ($p = 0.001$), inflammation ($p = 0.001$), abnormal calcification ($p = 0.007$), vascularization ($p = 0.015$), superficial assessment ($p = 0.001$), mid/deep zone assessment ($p = 0.002$), and overall assessment ($p = 0.003$). Healthy cartilage groups were found to score statistically higher than decellularized implants and empty defects in tissue morphology, surface architecture, abnormal calcification, and superficial assessment ($p < 0.05$ for all). Decellularized implants were not found to be statistically different from healthy cartilage samples for matrix staining, cell morphology, cell clustering, basal integration, tidemark formation, bone abnormalities, inflammation, vascularization, mid/deep assessment, and overall assessment ($p > 0.05$ for all), where empty defects were found to score significantly lower for all of this group ($p < 0.05$ for all). Location, the location–treatment interaction, and the animal random effect were not found to be significant for any measure ($p > 0.05$ for all) (Table 1).

MRI reveals morphological differences between samples

MRI analysis of cartilage showed morphological differences among samples, with distal decellularized implants qualitatively matching healthy cartilage samples, similar to histological analysis (Fig. 6). qMRI measures revealed an increase in $T_{1\rho}$ for empty defects compared to decellularized implants and healthy cartilage tissue, although the trend was not significant (treatment: $p = 0.369$, location: $p = 0.961$, interaction: $p = 0.732$). Likewise, increased T_2* magnitude and variability were increased in empty defects and the distal decellularized implants compared to healthy cartilage and the proximal decellularized implants, although the trend was not significant (treatment: $p = 0.246$, location: $p = 0.753$, interaction: $p = 0.634$). In addition, the random animal effect was not found to be significant for either measure ($p \geq 0.516$ for both).

Decellularized implants remain mechanically soft

Mechanical analysis of cartilage implants by AFM revealed a significant treatment effect for compressive modulus ($p < 0.001$) and friction coefficient ($p = 0.019$), but not

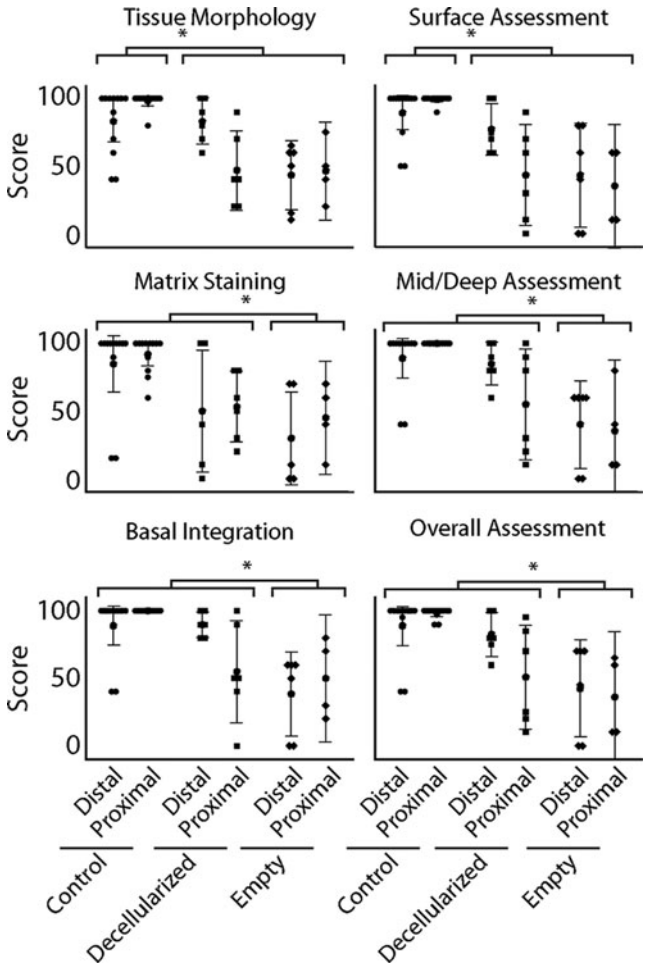

FIG. 5. Selected ICRS II measures of the state of the donor tissue after 3 months show significant differences between experimental groups, where distal decellularized implants were found to be most similar to control samples. Empty defect samples consistently show the greatest variability in all measures (complete list of ICRS II measures and statistical analysis, Table 1), consistently scoring lower than decellularized and control samples. For nearly all measures, distal decellularized implants scored the most similar to control samples with the least variability. (*$p<0.05$). ICRS II, International Cartilage Repair Society II.

surface roughness ($p=0.500$) (Fig. 7). For compressive modulus, healthy cartilage samples were found to be significantly higher than decellularized implants and empty defects ($p<0.05$). In addition, decellularized implants and empty defects were found to be statistically different than healthy cartilage samples for friction coefficient ($p<0.05$). Anatomical location was not found to be significant for any main effect. The interaction between treatment and anatomical location was found to be significant for friction coefficient ($p=0.002$) and compressive modulus ($p=0.002$), but not surface roughness ($p=0.455$) (Fig. 7). Significant differences between animals (random variable) were seen in RMS roughness ($p=0.018$) and compressive modulus ($p<0.001$), but not friction coefficient ($p=0.424$).

Discussion

This study showed cellular remodeling into a minimally modified, decellularized cartilage tissue *in vivo*. These results demonstrate the potential of dense decellularized articular cartilage in a physiologically and clinically relevant environment, at least in short-term (3 month) transplant studies, suggesting an increased utility of decellularized cartilage tissue over what has been previously reported.

Before implantation, SDS decellularization alters the ECM composition of the native tissue. Specifically, GAG content, as measured by DMMB analysis, was found to decrease by $\sim$47%. Partially correlated with GAG loss, collagen weight fraction was found to increase. However, it is unlikely that decellularization increased the net collagen content. The hydroxyproline assay utilized tissue samples that were normalized to weight. Due to the decrease in overall GAG content, the composition fraction of collagen per unit weight of tissue likely increased, resulting in a larger measured collagen weight fraction of the decellularized tissue. A primary purpose of this study was to minimize structural and biochemical alteration to the tissue as a result of decellularization, to understand cellular remodeling into near-native density tissue in a clinically relevant *in vivo* environment. It is important to note that, while the decellularization method utilized is relatively common across tissue types, with relatively few negative effects shown, a decrease in the GAG content may increase the porosity of the decellularized tissue and contribute to cellular remodeling. These data, showing a decrease

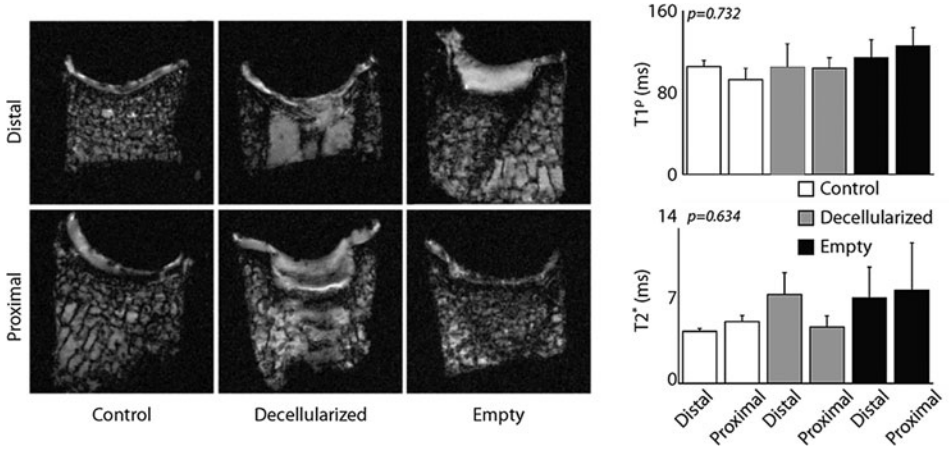

FIG. 6. Morphological, but not significant quantitative, differences were observed by magnetic resonance imaging in donor tissues after 3 months. Decellularized cartilage in the distal location qualitatively matched control samples. $T_{1\rho}$ and T_2* measures were generally increased in empty defects compared to control samples, although the trends were not significant ($p>0.246$).

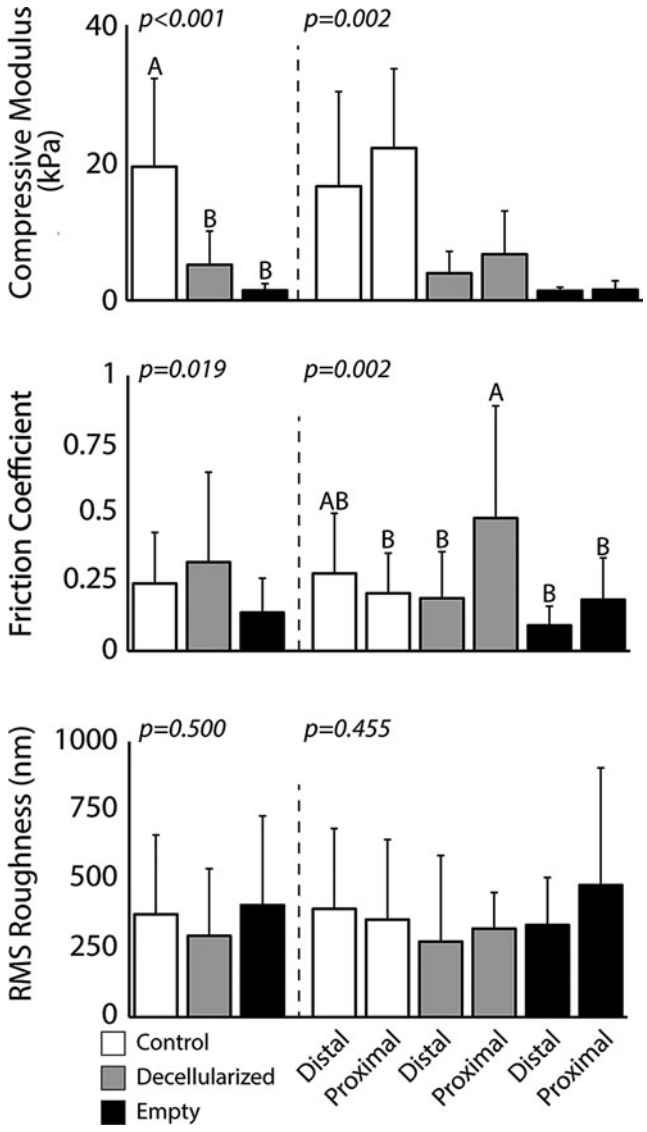

FIG. 7. atomic force microscopy analysis showed significant softening in donor tissue regions, but similar tribological properties between decellularized implants and control groups. Mean compressive modulus showed a near order-of-magnitude difference between control and experimental groups (decellularized implant and empty defect), while no effect was measured between anatomical locations. In addition, the friction coefficient was found to be significantly higher than empty defects, but similar to the control groups. No difference between any main effect was observed for surface roughness measures. Bars to the right of the *dashed line* show location-dependent trends. Bars with similar letters indicate groups that are not statistically different from one another.

in GAG content and, as a result, increase in wet-weight collagen content, are consistent with previous studies utilizing similar decellularization methods.[34]

Cellular remodeling was seen in decellularized implants and empty defect samples. Cells were found to remodel both sample groups at a nonsignificantly different level between the edge of the sample (closest to native chondrocyte source) and at the middle of the sample (furthest from the native chondrocyte source), suggesting equal remodeling. In addition, cells were shown to remodel into the tissue. However, it is important to note that cells were present at a lower viability and at a lower density than in the contralateral healthy cartilage samples. This suggests that over the 3-month period, cell remodeling and proliferation are slightly inhibited into the decellularized implants and defect zone, and the nonnative environment, and lack of repair mechanisms may contribute to the lower viability within these samples. Also, the decellularized implants and empty defects showed inferior compressive modulus compared to native cartilage, potentially causing high stress in the treatment samples and contributing to lower cell viability and density. However, to the authors' knowledge, this is the first report of *in vivo* cell remodeling into dense decellularized cartilage tissue beyond the surface of the tissue.

Quantitative and qualitative histological analysis of the implants showed that decellularized implants were similar in structure and cartilage-positive features compared to the empty defects. Most striking was the maintenance of depth-dependent structure, apparent reintegration, although with reduced GAG staining apparent in the decellularized implants. It is possible that a lack of cellular infiltration failed to restore GAG levels in decellularized cartilage to native levels *in vivo*. Conversely, empty defect samples were consistently fibrous, lacked depth-dependent structure, and did not exhibit an even surface for joint articulation. Quantitative ICRS II scores supported the increased quality of cartilage tissue, showing mostly no statistical significance between decellularized implant and healthy cartilage groups. Investigation of the data (Fig. 5) showed potential location differences for proximal decellularized implants, which have a high variability in scores for nearly all criteria. Distal decellularized implants, however, have relatively high scores and low variability for most ICRS II criteria, showing a general, although nonsignificant, trend of higher scores, suggesting maintenance of the structural and biochemical nature of native cartilage in distal decellularized implants over empty defects and the proximal decellularized implant group. Overall, the consistent trends seen are healthy cartilage samples, which are consistently high scoring in ICRS II criteria and histologically similar to structure and staining, as seen throughout the literature. Distal decellularized implants are also shown to be relatively high scoring and maintain many of the structural and staining features of native cartilage. Proximal decellularized implants show similar overall morphology to healthy cartilage and distal decellularized implants, but score lower for ICRS II criteria and stain less consistently with cartilage-positive Safranin-O. Empty defects were largely seen to be fibrous and relatively low scoring in ICRS II criteria.

MRI analysis of cartilage showed morphological differences among samples, with distal decellularized implants qualitatively matching healthy cartilage samples, consistent with histology (Fig. 6). qMRI measures revealed an increase in $T_{1\rho}$ for empty defects compared to decellularized implants and healthy cartilage tissue, although the trend was not significant (treatment: $p = 0.369$, location: $p = 0.961$, interaction: $p = 0.732$). Likewise, increased T_2* magnitude and variability were seen in empty defects and distal decellularized implants compared to healthy cartilage and proximal decellularized implants, although the trend was not significant (treatment: $p = 0.246$, location: $p = 0.753$, interaction: $p = 0.634$). Morphological differences were observed by standard (FLASH) MRI, and suggested that the structure of decellularized cartilage in the distal location was similar to healthy cartilage samples. However, this does not suggest that direct

noninvasive mechanical (i.e., functional) analysis[35,36] would remain indifferent to responses from treatment groups, as the sensitivity of qMRI for small population sizes, like what was studied here, has been questioned.[26] In some samples, decellularized cartilage in the proximal location appeared, by MRI, more similar to empty defects, suggesting a location-dependent bias for cartilage repair. Regional biomechanical and chemical measures are known to vary throughout the human and animal joints,[37,38] including the trochlear groove,[39] which may suggest a local influence of unique factors on *in vivo* repair.

Although qMRI measures did not reveal significant differences among samples, trends suggested increased the $T_{1\rho}$ and T_2* of empty defects compared to healthy cartilage. For qMRI, special care was taken to consistently align the depth direction axis of the osteochondral samples parallel to the main magnetic field (B0) of the MRI scanner, in light of known magic angle effects.[40] $T_{1\rho}$ measures, in our study, were slightly higher on average, although well within the ranges observed, compared to values obtained from humans *in vivo*,[41] and possibly due, in part, to our use of a larger spin lock frequency (of 1800 Hz vs. 500 Hz, respectively).[42] The increases in $T_{1\rho}$ that we observed in empty defects are consistent with cartilage pathology observed previously.[41,42] Increased T_2* measures over healthy cartilage were also consistent with previous animal studies of OA pathology.[43] While increasing the sample sizes for qMRI data may well lead to measured significant differences in the population, the large variability observed in our data suggests that qMRI analysis at the single-subject level is less reliable.

Mechanical analysis showed significant weakening in implant sites (decellularized and empty defect) compared to the healthy cartilage groups. The empty defect group showed histological formation of fibrocartilage and is consistent with clinical microfracture research.[44] The formation of fibrocartilage is well known to produce mechanically inferior tissue and is well documented as one of the primary limitations of the procedure.[44] In addition, decellularization of cartilage by SDS, as performed in this work, has also been shown to affect the mechanical properties of the tissue.[8,11,13,14] This is consistent with what is seen in the work performed herein. Interestingly, empty defect samples were found to have the lowest friction coefficient, but all treatment groups had similar surface roughness. This may suggest that a biochemical lubrication layer has formed in the empty defect tissue, but not the decellularized implant tissue. It is possible that decellularized implants, which more consistently conform to the joint structure, are more subject to shearing effects of the gait cycle than empty defects, which were shown to have an irregular structure inconsistent with the concave of the surrounding native tissue.

Conclusions

Decellularized cartilage implants have previously been shown to strongly inhibit cellular remodeling in both *in vitro* and *in vivo* settings. In this study, we showed cellular remodeling into a minimally modified decellularized allograft in an ovine model with a clinically relevant mechanical and biochemical environment. This study suggests that whole decellularized allografts, and potentially xenografts, may allow for cellular remodeling and potentially positive, long-term cartilage remodeling in a longer disease model. These data suggest that further study in established OA models using decellularized cartilage materials may benefit tissue integration and remodeling and should be further studied, especially in study durations designed to evaluate their long-term repair potential.

Acknowledgments

This work was supported, in part, by NIH grants R01 AR063712 and R21 AR066230 (C.P.N.), and NSF Graduate Research Fellowship Program under Grant No. DGE-0833366 (T.N.). The authors would like to thank Purdue Histology Laboratory and Cook Research Incorporated for histological processing, and Jonathan Henderson for assistance with cell viability experiments.

Disclosure Statement

No competing financial interests exist.

References

1. Chen, C.C., Liao, C.H., Wang, Y.H., Hsu, Y.M., Huang, S.H., Chang, C.H., and Fang, H.W. Cartilage fragments from osteoarthritic knee promote chondrogenesis of mesenchymal stem cells without exogenous growth factor induction. J Orthop Res **30,** 393, 2012.
2. Cheng, C.W., Solorio, L.D., and Alsberg, E. Decellularized tissue and cell-derived extracellular matrices as scaffolds for orthopaedic tissue engineering. Biotechnol Adv **32,** 462, 2014.
3. Chen, Y.C., Chen, R.N., Jhan, H.J., Liu, Z., Ho, H.O., Mao, Y., Kohn, J., and Sheu, M.T. Development and characterization of acellular extracellular matrix scaffolds from porcine menisci for use in cartilage tissue engineering. Tissue Eng Part C Methods **21,** 971, 2015.
4. Bitton, R. The economic burden of osteoarthritis. Am J Manag Care **15,** S230, 2009.
5. Quinn, T.M., Grodzinsky, A.J., Hunziker, E.B., and Sandy, J.D. Effects of injurious compression on matrix turnover around individual cells in calf articular cartilage explants. J Orthop Res **16,** 490, 1998.
6. Chang, C.H., Chen, C.C., Liao, C.H., Lin, F.H., Hsu, Y.M., and Fang, H.W. Human acellular cartilage matrix powders as a biological scaffold for cartilage tissue engineering with synovium-derived mesenchymal stem cells. J Biomed Mater Res A **102,** 2248, 2014.
7. Philp, D., Chen, S.S., Fitzgerald, W., Orenstein, J., Margolis, L., and Kleinman, H.K. Complex extracellular matrices promote tissue-specific stem cell differentiation. Stem Cells **23,** 288, 2005.
8. Novak, T., Seelbinder, B., Twitchell, C.M., van Donkelaar, C.C., Voytik-Harbin, S.L., and Neu, C.P. Mechanisms and microenvironment investigation of cellularized high density gradient collagen matrices via densification. Adv Funct Mater **26,** 2617, 2016.
9. Novak, T., Seelbinder, B., Twitchell, C.M., Voytik-Harbin, S.L., and Neu, C.P. Dissociated and reconstituted cartilage microparticles in densified collagen induce local hMSC Differentiation. Adv Funct Mater **26,** 5427, 2016.
10. Novak, T., Voytik-Harbin, S.L., and Neu, C.P. Cell encapsulation in a magnetically aligned collagen-GAG copolymer microenvironment. Acta Biomater **11,** 274, 2015.
11. Elder, B.D., Eleswarapu, S.V., and Athanasiou, K.A. Extraction techniques for the decellularization of tissue

engineered articular cartilage constructs. Biomaterials **30,** 3749, 2009.
12. Peretti, G.M., Randolph, M.A., Caruso, E.M., Rossetti, F., and Zaleske, D.J. Bonding of cartilage matrices with cultured chondrocytes: an experimental model. J Orthop Res **16,** 89, 1998.
13. Cheng, N.C., Estes, B.T., Awad, H.A., and Guilak, F. Chondrogenic differentiation of adipose-derived adult stem cells by a porous scaffold derived from native articular cartilage extracellular matrix. Tissue Eng Part A **15,** 231, 2009.
14. Diekman, B.O., Rowland, C.R., Lennon, D.P., Caplan, A.I., and Guilak, F. Chondrogenesis of adult stem cells from adipose tissue and bone marrow: induction by growth factors and cartilage-derived matrix. Tissue Eng Part A **16,** 523, 2010.
15. Peretti, G.M., Randolph, M.A., Villa, M.T., Buragas, M.S., and Yaremchuk, M.J. Cell-based tissue-engineered allogeneic implant for cartilage repair. Tissue Eng **6,** 567, 2000.
16. Yang, Q., Peng, J., Guo, Q., Huang, J., Zhang, L., Yao, J., Yang, F., Wang, S., Xu, W., Wang, A., and Lu, S. A cartilage ECM-derived 3-D porous acellular matrix scaffold for in vivo cartilage tissue engineering with PKH26-labeled chondrogenic bone marrow-derived mesenchymal stem cells. Biomaterials **29,** 2378, 2008.
17. Harada, T., Swift, J., Irianto, J., Shin, J.W., Spinler, K.R., Athirasala, A., Diegmiller, R., Dingal, P.C., Ivanovska, I.L., and Discher, D.E. Nuclear lamin stiffness is a barrier to 3D migration, but softness can limit survival. J Cell Biol **204,** 669, 2014.
18. Wolf, K., Te Lindert, M., Krause, M., Alexander, S., Te Riet, J., Willis, A.L., Hoffman, R.M., Figdor, C.G., Weiss, S.J., and Friedl, P. Physical limits of cell migration: control by ECM space and nuclear deformation and tuning by proteolysis and traction force. J Cell Biol **201,** 1069, 2013.
19. Schwarz, S., Koerber, L., Elsaesser, A.F., Goldberg-Bockhorn, E., Seitz, A.M., Dürselen, L., Ignatius, A., Walther, P., Breiter, R., and Rotter, N. Decellularized cartilage matrix as a novel biomatrix for cartilage tissue-engineering applications. Tissue Eng Part A **18,** 2195, 2012.
20. Kang, H., Peng, J., Lu, S., Liu, S., Zhang, L., Huang, J., Sui, X., Zhao, B., Wang, A., Xu, W., Luo, Z., and Guo, Q. In vivo cartilage repair using adipose-derived stem cell-loaded decellularized cartilage ECM scaffolds. J Tissue Eng Regen Med **8,** 442, 2014.
21. Gong, Y.Y., Xue, J.X., Zhang, W.J., Zhou, G.D., Liu, W., and Cao, Y. A sandwich model for engineering cartilage with acellular cartilage sheets and chondrocytes. Biomaterials **32,** 2265, 2011.
22. Benders, K.E., van Weeren, P.R., Badylak, S.F., Saris, D.B., Dhert, W.J., and Malda, J. Extracellular matrix scaffolds for cartilage and bone regeneration. Trends Biotechnol **31,** 169, 2013.
23. Hollander, A.P., Heathfield, T.F., Webber, C., Iwata, Y., Bourne, R., Rorabeck, C., and Poole, A.R. Increased damage to type II collagen in osteoarthritic articular cartilage detected by a new immunoassay. J Clin Invest **93,** 1722, 1994.
24. Handley, C.J., and Buttle, D.J. Assay of proteoglycan degradation. Methods Enzymol **248,** 47, 1995.
25. Mainil-Varlet, P., Van Damme, B., Nesic, D., Knutsen, G., Kandel, R., and Roberts, S. A new histology scoring system for the assessment of the quality of human cartilage repair: ICRS II. Am J Sports Med **38,** 880, 2010.
26. Chan, D.D., and Neu, C.P. Probing articular cartilage damage and disease by quantitative magnetic resonance imaging. J R Soc Interface **10,** 20120608, 2013.
27. Hesper, T., Hosalkar, H.S., Bittersohl, D., Welsch, G.H., Krauspe, R., Zilkens, C., and Bittersohl, B. T2* mapping for articular cartilage assessment: principles, current applications, and future prospects. Skeletal Radiol **43,** 1429, 2014.
28. Chan, S.M., Neu, C.P., Duraine, G., Komvopoulos, K., and Reddi, A.H. Atomic force microscope investigation of the boundary-lubricant layer in articular cartilage. Osteoarthritis Cartilage **18,** 956, 2010.
29. Chan, S.M., Neu, C.P., Komvopoulos, K., and Reddi, A.H. Dependence of nanoscale friction and adhesion properties of articular cartilage on contact load. J Biomech **44,** 1340, 2011.
30. Hutter, J.L., and Bechhoefer, J. Calibration of atomic-force microscope tips. Rev Sci Instrum **64,** 1868, 1993.
31. Horcas, I., Fernandez, R., Gomez-Rodriguez, J.M., Colchero, J., Gomez-Herrero, J., and Baro, A.M. WSXM: a software for scanning probe microscopy and a tool for nanotechnology. Rev Sci Instrum **78,** 013705, 2007.
32. Cain, R.G., Biggs, S., and Page, N.W. Force calibration in lateral force microscopy. J Colloid Interface Sci **227,** 55, 2000.
33. Hertz, H. On the contact of elastic solids. J. Reine Angew. Math. **92,** 156, 1882.
34. Utomo, L., Pleumeekers, M.M., Nimeskern, L., Nürnberger, S., Stok, K.S., Hildner, F., and van Osch, G.J. Preparation and characterization of a decellularized cartilage scaffold for ear cartilage reconstruction. Biomed Mater **10,** 015010, 2015.
35. Butz, K.D., Chan, D.D., Nauman, E.A., and Neu, C.P. Stress distributions and material properties determined in articular cartilage from MRI-based finite strains. J Biomech **44,** 2667, 2011.
36. Chan, D.D., Neu, C.P., and Hull, M.L. In situ deformation of cartilage in cyclically loaded tibiofemoral joints by displacement-encoded MRI. Osteoarthritis Cartilage **17,** 1461, 2009.
37. Neu, C.P., Khalafi, A., Komvopoulos, K., Schmid, T.M., and Reddi, A.H. Mechanotransduction of bovine articular cartilage superficial zone protein by transforming growth factor beta signaling. Arthritis Rheum **56,** 3706, 2007.
38. Neu, C.P., Reddi, A.H., Komvopoulos, K., Schmid, T.M., and Di Cesare, P.E. Increased friction coefficient and superficial zone protein expression in patients with advanced osteoarthritis. Arthritis Rheum **62,** 2680, 2010.
39. Nugent-Derfus, G.E., Takara, T., O'neill, J.K., Cahill, S.B., Görtz, S., Pong, T., Inoue, H., Aneloski, N.M., Wang, W.W., Vega, K.I., Klein, T.J., Hsieh-Bonassera, N.D., Bae, W.C., Burke, J.D., Bugbee, W.D., and Sah, R.L. Continuous passive motion applied to whole joints stimulates chondrocyte biosynthesis of PRG4. Osteoarthritis Cartilage **15,** 566, 2007.
40. Akella, S.V., Regatte, R.R., Wheaton, A.J., Borthakur, A., and Reddy, R. Reduction of residual dipolar interaction in cartilage by spin-lock technique. Magn Reson Med **52,** 1103, 2004.

41. Singh, A., Haris, M., Cai, K., Kogan, F., Hariharan, H., and Reddy, R. High resolution T1ρ mapping of in vivo human knee cartilage at 7T. PLoS One **9,** e97486, 2014.
42. Fenty, M.C., Dodge, G.R., Kassey, V.B., Witschey, W.R., Borthakur, A., and Reddy, R. Quantitative cartilage degeneration associated with spontaneous osteoarthritis in a guinea pig model. J Magn Reson Imaging **35,** 891, 2012.
43. Tsai, P.H., Lee, H.S., Siow, T.Y., Chang, Y.C., Chou, M.C., Lin, M.H., Lin, C.Y., Chung, H.W., and Huang, G.S. Sequential change in T2* values of cartilage, meniscus, and subchondral bone marrow in a rat model of knee osteoarthritis. PLoS One **8,** e76658, 2013.
44. Huey, D.J., Hu, J.C., and Athanasiou, K.A. Unlike bone, cartilage regeneration remains elusive. Science **338,** 917, 2012.

Address correspondence to:
Corey P. Neu, PhD
Department of Mechanical Engineering
University of Colorado Boulder
1111 Engineering Drive
UCB 427
Boulder, CO 80304

E-mail: cpneu@colorado.edu

Received: May 16, 2016
Accepted: September 13, 2016
Online Publication Date: October 24, 2016